

## Surface complexation of nickel on iron and aluminum oxides: A comparative study with single and dual site clays

Anushka Upamali Rajapaksha<sup>a</sup>, Meththika Vithanage<sup>a,\*</sup>, R. Weerasooriya<sup>c</sup>, C.B. Dissanayake<sup>b</sup>

<sup>a</sup> Chemical and Environmental Systems Modeling Research Group, Institute of Fundamental Studies, Hantana Road, Kandy 20000, Sri Lanka

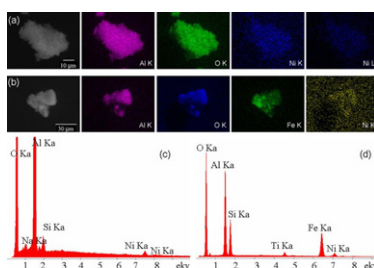
<sup>b</sup> Institute of Fundamental Studies, Hantana Road, Kandy 20000, Sri Lanka

<sup>c</sup> Department of Soil Science, University of Peradeniya, Sri Lanka

### HIGHLIGHTS

► Surface complexation modeling of Ni on single/dual site clays was studied. ► Ni adsorption capacity varied in the order of gibbsite > laterite > NRE > goethite. ► High affinity of Ni was observed to AlOH surface sites of all clays.

### GRAPHICAL ABSTRACT



### ARTICLE INFO

#### Article history:

Received 5 April 2012

Received in revised form 29 April 2012

Accepted 1 May 2012

Available online 7 May 2012

#### Keywords:

Diffuse double layer model

Gibbsite

Laterite

Goethite

Natural red earth

### ABSTRACT

Ni adsorption on various single and dual site clays (gibbsite, goethite, natural red earth and laterite) was determined using batch experiments as a function of pH, background electrolyte concentration and adsorbate loading. The experimental data was quantified by 2-pK surface complexation modeling using monodentate and bidentate surface reactions. Gibbsite and laterite showed higher retention of Ni compared to natural red earth (NRE) and goethite indicating high affinity to  $\equiv\text{AlOH}$  surface sites of all clays. The maximum adsorption density of  $9.0 \times 10^{-5} \text{ mol m}^{-2}$  was reported for gibbsite. All four sorbents showed a negligible variation with ionic strength. The Ni adsorption capacity, i.e.,  $\Gamma_{\text{Ni}}$ , varied with the type of sorbents used in accordance with the following order:  $\Gamma_{\text{Gibbsite}} \text{ Ni} > \Gamma_{\text{Laterite}} \text{ Ni} > \Gamma_{\text{NRE}} > \Gamma_{\text{Goethite}} \text{ Ni}$ . In all cases, the estimated Gibb's free energy parameter showed that the Ni(II) adsorption was spontaneous.

© 2012 Elsevier B.V. All rights reserved.

### 1. Introduction

Natural substances, such as nickel and most of its compounds, have existed on the earth for billions of years and due to weathering and other pedogenic processes, nickel occurs naturally in soils, sediments and waters. However, their existence is not always ecotoxic since weathering cannot supply enough bioavailable Ni to the environment. In some cases, nickel rich soils such as serpentine and nickel laterite can release high concentrations of bioavailable and exchangeable Ni to the local environment [1–3]. Anthropogenic

substances that are synthesized and released represent a far more serious challenge for ecological systems as well as for human beings than by natural substances merely because artificial substances are new additions to the environment and organisms may not have developed managing mechanisms for them. Excessive Ni concentrations may cause cancer. Nickel carcinogenicity has been reported in animals and humans [4,5]. Since, Ni is a toxic metal widely used in many common industries such as electroplating, zinc base casting and storage batteries [6,7] which can release bioavailable and exchangeable Ni to the environment as Ni rich soils do, it is important to find a better removal technology.

Several adsorbents such as kaolinite [8–10], montmorillonite [8,9,11], iron oxide [12], goethite and hematite [13], peat [14], bentonite [15], peanut hull ash [16], ZnO [17], charcoal [18] and rice

\* Corresponding author. Tel.: +94 812232002; fax: +94 812232131.

E-mail address: [meththikavithanage@gmail.com](mailto:meththikavithanage@gmail.com) (M. Vithanage).

husk ash [19] have been tested for Ni removal in different scales. However, only few studies have been carried out to compare the adsorption efficiencies [13,18,20–22]. It has been reported that montmorillonite showed the greatest adsorption of Ni as compared to kaolinite from pH 1 to 8 and adsorption increased with increase of pH [8]. A similar behavior with pH was recorded for goethite and hematite [13]. The best pH for Ni adsorption on natural iron oxide coated sand has been reported as 7.0 [12]. However for bentonite the maximum adsorption was recorded at pH 8–10 [15].

Most of these Ni sorption studies have been conducted on single site clay minerals such as montmorillonite or goethite. Only very few experiments have been reported on mixtures of sorbents which give dual sites for Ni adsorption [23]. However, when there is a mixture of sites, metal sorption cannot be estimated by the distribution coefficients of different single clay minerals [23,24] and hence, surface complexation modeling (SCM) plays an important role in such cases. It has been previously demonstrated that modeling alone cannot distinguish between plausible adsorption complexes [25,26] and that spectroscopic investigations play an important role. To our knowledge there have been no direct spectroscopic investigations of Ni(II) adsorption on clay minerals such as gibbsite. This knowledge gaps provide an excellent platform for the calculation of interfacial properties of single and dual site clays for Ni adsorption.

Previous researchers have used different models for speciation and sorption calculations of nickel adsorption on different materials [9,11,20,23] and many have used the diffuse double layer model (DDLDM). However, not many studies compared Ni adsorption on minerals with single and dual site systems. In this study, modeling sorption of Ni was carried out using the DDLDM and 2-pK approach using non-linear least square fit, FITEQL32. The 2-pK approach is widely used for metal (hydroxyl) oxides where the surface is hydroxylated in two steps,  $\equiv\text{SOH} + \text{H}^+ \rightarrow \equiv\text{SOH}_2^+$  and  $\equiv\text{SOH} \rightarrow \equiv\text{SO}^- + \text{H}^+$ . The DDLDM was selected since it is simple, capable of handling several surface sites simultaneously, easy to compare with data from other studies due to the frequent use and its ability to use Gouy–Chapman theory. Therefore, DDLDM gives the optimal conditions for the estimation of surface protolysis constants [27].

Therefore, the present paper aims to examine (i) Ni sorption to single as well as dual site clays (Al dominant, Fe dominant and both Al and Fe rich sorbents) as adsorbents for removal of Ni from aqueous solutions and compare the capacities, (ii) study the effect of solution pH, (iii) examine the effect of ionic strength on adsorption (iv) determine the adsorption capacity through isotherm models (i.e., Langmuir, Freundlich, Hill, Redlich Peterson models and their regression analysis) and (v) to understand the mechanisms of adsorption through surface complexation modeling and FT-IR. Gibbsite and goethite were selected as the single site sorbent for Al and Fe while Natural Red Earth (NRE) and laterite, were used as the sorbents with dual sites for this study. Although many types of clays have been tested for Ni adsorption these clay minerals have not been examined much for Ni adsorption, and for surface complexation modeling [23]. Since the surface complexation models are based on actual surface species, we believe our results will be more reliable when applied to modeling uptake of Ni in complex natural systems.

## 2. Materials and methods

### 2.1. Adsorbents and chemicals

Gibbsite used was obtained from ALCOA (Australia) and goethite synthesis was carried out based on the literature [28]. Laterite and NRE was obtained from South-Western and North-Western parts

**Table 1**

Surface area of sorbents and equilibrium speciation constants of Ni used in the DDLDM calculations.

Parameter/reaction	log K	Reference
Reactions		
$\text{Ni}^{2+} + \text{H}_2\text{O} \rightarrow \text{NiOH}^+ + \text{H}^+$	−9.9	[23]
$\text{Ni}^{2+} + 2\text{H}_2\text{O} \rightarrow \text{Ni}(\text{OH})_2^0 + 2\text{H}^+$	−19	[23]
$4\text{Ni}^{2+} + 4\text{H}_2\text{O} \rightarrow \text{Ni}_4(\text{OH})_4^{4-} + 4\text{H}^+$	−27.7	[23]
Surface area (m <sup>2</sup> /g)		
Gibbsite	13	[44]
Goethite	95	[30]
Laterite	24	[34]
NRE	350	[30]

of Sri Lanka from the deposits, respectively. The physicochemical properties of all sorbents are given in Table 1. Synthetic goethite was characterized by FT-IR.

Natural red earth is considered as an iron-coated quartz sand with ilmenite and magnetite in minor amounts [29]. It is the direct weathering product of limestone, which is mined for the cement industry. X-ray diffraction (XRD) analysis indicated that the sand mainly consists of silica, by exhibiting the characteristic peak of 3.340 for  $\equiv\text{SiO}_2$  phase [30]. However, X-ray fluorescence analysis showed that other than silica,  $\text{Al}_2\text{O}_3$  and  $\text{Fe}_2\text{O}_3$  are present in considerable amounts (20 and 12% respectively). Peaks in XRD spectrum showed the presence of hematite, magnetite and gibbsite, no any dominance observed. It may be due to the amorphous coating of Al and Fe in the composition [31].

Laterites are the common weathering products of rocks under tropical climatic conditions. Their composition is based on the nature of the parent rock, depth and climatic conditions. Laterites show divergent chemical compositions [32] and mineralogically, it is essentially a mixture of varying proportions of goethite, hematite, kaolin and gibbsite due to chemical alterations in weathering [32,33]. Laterite used in this study was characterized by XRF, XRD, FTIR and consist of  $\text{SiO}_2$ : 21.13,  $\text{Al}_2\text{O}_3$ : 29.21,  $\text{Fe}_2\text{O}_3$ : 40.90, CaO: 2.22, MgO: 0.21,  $\text{SO}_3$ : 0.12,  $\text{K}_2\text{O}$ : 0.02 and  $\text{Na}_2\text{O}$ : 0.01% [34].

Similar grain size (<63  $\mu\text{m}$ ) was used for all the 4 adsorbents. All the other chemicals used in this study were of analytical reagent (AR) grade from Fluka (Switzerland). Stock solutions of Ni(II) of 1000  $\text{mg L}^{-1}$  were made by dissolving the exact amount of  $\text{Ni}(\text{NO}_3)_2 \cdot 6\text{H}_2\text{O}$  in distilled deionized water.

### 2.2. Adsorption edges and isotherm study

Unless otherwise mentioned, all adsorption experiments were conducted at 25 °C under high purity (99.996%)  $\text{N}_2$  purged conditions to minimize atmospheric contamination of  $\text{CO}_2$ . The effect of pH on the sorption was studied by adjusting the pH in the range of 4–9. In these experiments, the adsorbent concentration was kept at 5 g/L of solution containing  $1.709 \times 10^{-4}$  M Ni(II) at 25 °C. Altogether 12 experiments were carried out to describe Ni sorption to single and dual sorbents as a function of pH in the range 4.0–9.0 with the same initial Ni and sorbent concentrations. Control samples without the adsorbent and replicates were conducted for each experiment. The pH was adjusted with 0.1 M  $\text{HNO}_3$  or NaOH. This experiment was carried out for 3 different electrolyte concentrations, 0.1, 0.01 and 0.001 M. Sodium nitrate was used as the ionic strength adjuster. Sorption investigations were conducted as batch experiments in 50 ml polyethylene (PE) bottles at room temperature. Preliminary experiments showed that Ni sorption to most sorbents reached equilibrium within a few hours of agitation. Therefore 24 h of shaking was used as contact time in all sorption experiments. Scanning electron microscope (SEM) and energy dispersive X-ray analysis (EDAX) (EFI QUANTA-200) were carried out for the materials with the highest adsorptive capacity.

**Table 2**  
Reactions stoichiometries of surface species, acidity constants and optimized best estimates of intrinsic surface complexation constants of four sorbents.

	log K	Reference		
<b>Gibbsite</b>				
$\equiv\text{AlOH} + \text{H}^+ \rightarrow \text{AlOH}_2^+$	4.70	[48]		
$\equiv\text{AlOH} \rightarrow \text{AlO}^- + \text{H}^+$	-8.7	[48]		
Surface reactions – Gibbsite	0.1 M	0.01 M	0.001 M	Weighted mean <sup>a</sup>
$\equiv\text{AlOH} + \text{Ni}^{2+} \rightarrow \text{AlONi}^+ + \text{H}^+$	-12.85	-11.85	-10.06	-11.63
$\equiv 2\text{AlOH} + \text{Ni}^{2+} \rightarrow (\text{AlO})_2\text{Ni}$	-4.76	-4.31	-2.98	-4.26
<b>Goethite</b>				
$\equiv\text{FeOH} + \text{H}^+ \rightarrow \text{FeOH}_2^+$	7.10	[49]		
$\equiv\text{FeOH} \rightarrow \text{FeO}^- + \text{H}^+$	-9.64	[49]		
Surface reactions – Goethite	0.1 M	0.01 M	0.001 M	Weighted mean <sup>a</sup>
$\equiv\text{FeOH} + \text{Ni}^{2+} \rightarrow \text{FeONi}^+ + \text{H}^+$	-4.10	-4.50	-3.93	-4.38
$\equiv 2\text{FeOH} + \text{Ni}^{2+} \rightarrow (\text{FeO})_2\text{Ni}$	7.88	7.29	7.45	7.52
<b>Laterite</b>				
$\equiv\text{FeOH} + \text{H}^+ \rightarrow \text{FeOH}_2^+$	7.94	[34]		
$\equiv\text{AlOH} + \text{H}^+ \rightarrow \text{AlOH}_2^+$	6.67	[34]		
$\equiv\text{FeOH} \rightarrow \text{FeO}^- + \text{H}^+$	-4.24	[34]		
$\equiv\text{AlOH} \rightarrow \text{AlO}^- + \text{H}^+$	-6.73	[34]		
Surface reactions – Laterite	0.1 M	0.01 M	0.001 M	Weighted mean <sup>a</sup>
$\equiv\text{FeOH} + \text{Ni}^{2+} \rightarrow \text{FeONi}^+ + \text{H}^+$	-0.76	-0.72	-0.72	-0.74
$\equiv 2\text{FeOH} + \text{Ni}^{2+} \rightarrow (\text{FeO})_2\text{Ni}$	-0.24	-0.41	-0.53	-0.41
$\equiv\text{AlOH} + \text{Ni}^{2+} \rightarrow \text{AlONi}^+ + \text{H}^+$	-3.19	-3.09	-3.31	-3.21
$\equiv 2\text{AlOH} + \text{Ni}^{2+} \rightarrow (\text{AlO})_2\text{Ni}$	-2.56	-2.80	-2.51	-2.73
<b>NRE</b>				
$\equiv\text{FeOH} + \text{H}^+ \rightarrow \text{FeOH}_2^+$	4.74	[30]		
$\equiv\text{AlOH} + \text{H}^+ \rightarrow \text{AlOH}_2^+$	7.22	[30]		
$\equiv\text{FeOH} \rightarrow \text{FeO}^- + \text{H}^+$	-9.03	[30]		
$\equiv\text{AlOH} \rightarrow \text{AlO}^- + \text{H}^+$	-9.32	[30]		
Surface reactions – NRE	0.1 M	0.01 M	0.001 M	Weighted mean <sup>a</sup>
$\equiv\text{FeOH} + \text{Ni}^{2+} \rightarrow \text{FeONi}^+ + \text{H}^+$	-0.55	-0.35	-0.41	-0.47
$\equiv 2\text{FeOH} + \text{Ni}^{2+} \rightarrow (\text{FeO})_2\text{Ni}$	3.06	2.99	1.66	2.38
$\equiv\text{AlOH} + \text{Ni}^{2+} \rightarrow \text{AlONi}^+ + \text{H}^+$	-3.05	-2.90	-3.37	-3.10
$\equiv 2\text{AlOH} + \text{Ni}^{2+} \rightarrow (\text{AlO})_2\text{Ni}$	-4.43	-3.02	-3.66	-3.88

<sup>a</sup> Weighted averages were calculated using  $\log K = \sum \omega_i (\log K)_i$ , where  $\omega_i = (1/\sigma_{\log K})_i / \sum (1/\sigma_{\log K})_i$ , where  $\sigma_{\log K}$  is the standard deviation obtained from FITEQL calculations.

Nickel adsorption isotherms were conducted in 0.01 M  $\text{NaNO}_3$  solution, at  $\text{pH} \approx 7.0$  and at  $25^\circ\text{C}$  based on the adsorption edge experiments. The pH adjustment was made with 0.1 M NaOH and 0.1 M  $\text{HNO}_3$  solution. The initial Ni concentrations varied between  $1.709 \times 10^{-5}$  and  $1.709 \times 10^{-3}$  M. The 500 ml of 5 g/L solid suspensions were hydrated for 24 h, and thereafter 20 ml aliquots were sampled into polypropylene centrifuge tubes. Desired amounts of Ni were spiked into the system, equilibrated for 24 h. The sorbed mass of Ni was calculated as the difference between the initial and final Ni concentrations determined by atomic absorption spectrophotometry (AAS) (GBC 933A AAS) in the supernatant after centrifugation at 2500 for 20 min.

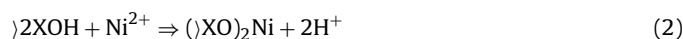
### 2.3. FTIR determination

FT-IR measurements were conducted using Nicolet 6700 spectrometer. The Fourier transform infrared spectrograms of vacuum dried adsorbents samples pellets prepared with fused-KBr, were obtained with a resolution of  $1 \text{ cm}^{-1}$  between 4000 and  $400 \text{ cm}^{-1}$ . Pellets were prepared with adsorbents with an equal amount of KBr for all samples at a 10:1 ratio. The spectra were analyzed using OMNIC version 7.3 software.

### 2.4. Modeling sorption of Ni

The surface protolysis constants values for the sorbents were fixed at the reported values in the literature (Table 2). Cation adsorption is analogous to metal hydrolysis in solution [35] and in this study,  $\text{Ni}^{2+}$  ions form either monodentate surface complexes

(reaction (1)) or bidentate surface complexes (reaction (2)) resulting in the release of  $\text{H}^+$  from the surface.



In our study, the constants for surface complexation of Ni to the mineral surface sites (reactions (1) and (2)) were estimated from sorption studies as a function of pH using FITEQL. Specific adsorption of Ni(II) to gibbsite was assumed only to consist of complexation to aluminol edge sites due to their higher affinity for positively charged ion. Since the sorption batches were purged with  $\text{N}_2$  during preparation, Ni carbonate speciation reactions and carbonate surface reactions were not accounted. Solution speciation equilibrium applied in parameter estimation and model calculations are listed in Tables 1 and 2.

## 3. Results and discussion

Gibbsite and laterite showed the highest adsorption at pH 7.5 and their SEM-EDAX images are shown in Fig. 1. Elemental composition of the sorbent was determined from its EDAX spectra (Fig. 1c and d). The EDAX spectrum showed the dominance of alumina in both materials, iron oxides and titanium in the laterite composition which can be attributed to the clayey nature of this sorbent. Elemental mapping demonstrated the distribution of elements on the grain including sorbed Ni. From the elemental dot mapping, it was noted that Ni is prominently seen where Al sites are seen. These results indicate that  $\equiv\text{AlO}^-$  sites attract Ni better than  $\equiv\text{FeO}^-$  sites.

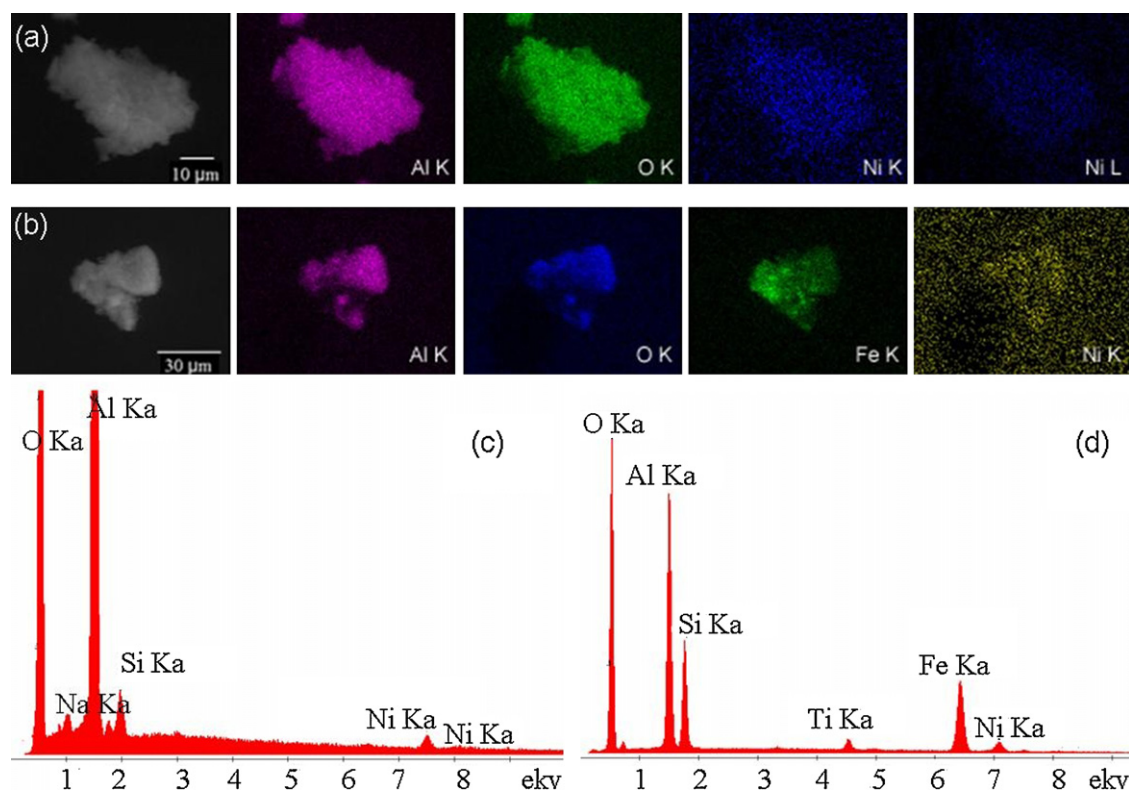


Fig. 1. SEM-EDAX elemental mapping and spectra of Ni loaded gibbsite (a and c) and laterite (b and d).

### 3.1. Sorption as a function of pH and ionic strength

#### 3.1.1. Experimental results and surface complexation modeling

Both single and dual site clay minerals have exhibited a sigmoid adsorption pattern when compared to each other; however, their adsorption capacities are different (Figs. 2 and 3). Up to pH 6, sorption showed a weak adsorption for all adsorbents except NRE. Beyond pH 6, Ni adsorption increased with increasing pH exhibiting the strong sorption on mineral surfaces of gibbsite, laterite and goethite while NRE showed increasing adsorption from pH 4.0 in a slow rate up to pH 6.8. Adsorption increased 4–5-folds with the pH increase from 6.0 to 8.0 with maximum adsorption at pH > 7.5. In the pH range where the positively charged sites of the adsorbents become negative (around the zero point charge of the sorbents and above), adsorption increased sharply. Negative surface charge

progressively adsorbs positive charged metal ions. The experimental results are shown in Figs. 2 and 3 (by symbols). Adsorption capacities were in the order: gibbsite > laterite > NRE > goethite.

Considering the solution chemistry, the chemical species of nickel was considered. The solubility product,  $K_{sp}$  of  $\text{Ni}(\text{OH})_2$  is about  $5.48 \times 10^{-16}$  at 298 K [36]. Ni(II) is removed by both adsorption as well as precipitation but in our studies, the total  $[\text{Ni}^{2+}]$  is less than the amount needed for the  $\text{Ni}(\text{OH})_2$  precipitation up to pH 9.5 which shows the unsaturated condition with respect to  $\text{Ni}(\text{OH})_2$  precipitation.

The effect of ionic strength on Ni adsorption was determined for the same Ni concentration used for pH dependency and shows no dependence on ionic strength concentration although the ionic strength varied to 100-fold. According to the results, the point of inflection ( $\text{pH}_{50\%}$  – pH corresponds to 50% adsorption) in laterite

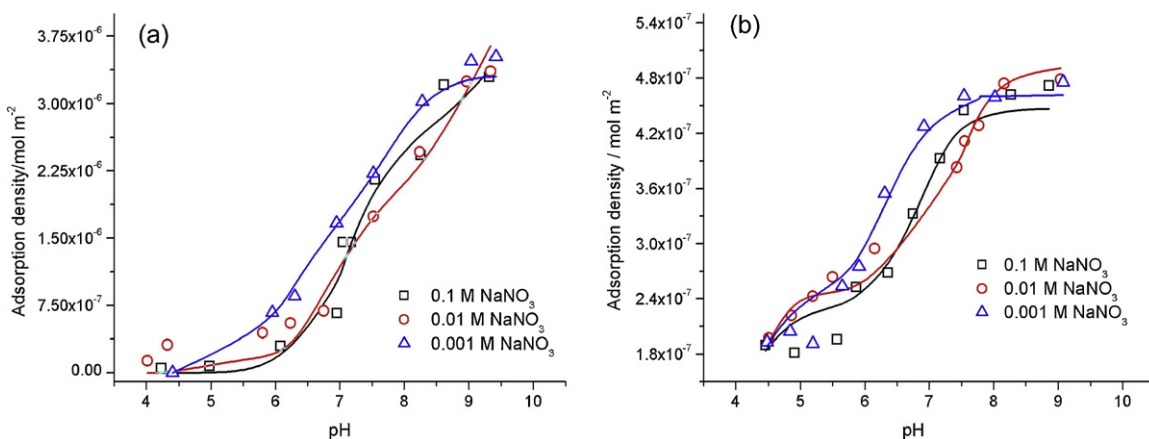
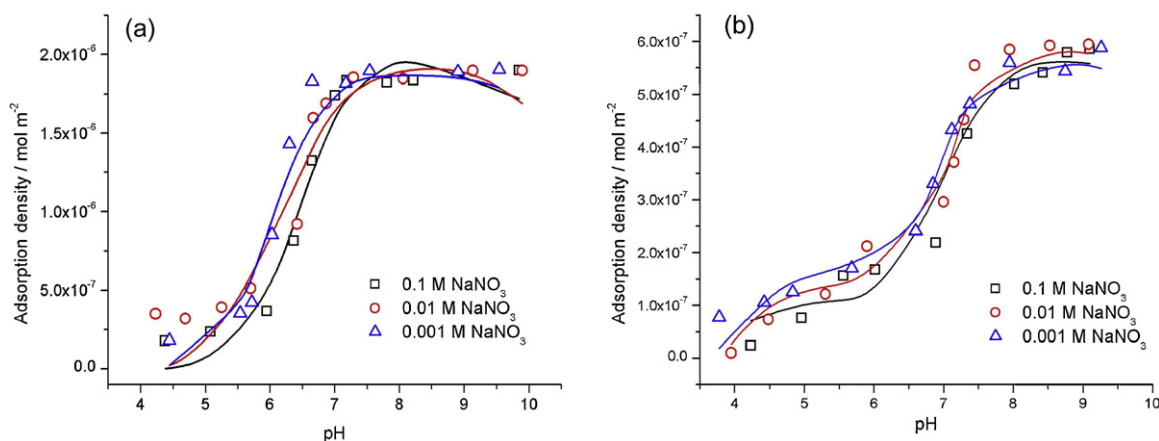


Fig. 2. Variation of Ni adsorption density as a function of pH and electrolyte concentration for single site clays; gibbsite (a) and goethite (b). Initial Ni concentration is  $1.709 \times 10^{-4}$  M. Lines are FITEQL model calculations while symbols represent experimental data.



**Fig. 3.** Variation of Ni adsorption density as a function of pH and electrolyte concentration for dual site clays; laterite (a) and NRE (b). Initial Ni concentration is  $1.709 \times 10^{-4}$  M. Lines are FITEQL model calculations while symbols represent experimental data.

was found at pH 6.20 for 0.1 M NaNO<sub>3</sub> and this point of inflection was slightly different from 0.01 M (pH 6.42) and 0.001 M (pH 6.51) NaNO<sub>3</sub>. In physical adsorption, outer-sphere complexes show a strong dependence on the ionic strength and yield distinctly separated adsorption edges for different ionic strengths, while such an observation cannot be made for inner-sphere complexes since the adsorption is stronger compared to physisorption [37]. The pH<sub>50%</sub> differs only by about 0.2–0.4 pH units for the 100-fold variation of ionic strength for all the adsorbents studied here. This gives a strong indication for the surface, possibly an inner sphere complex formation.

The best DDLM fit for Ni was specified by the parameters for reactions given in Table 1. The intrinsic surface complexation constants resulted by DDLM are given in Table 2. The inclusion of monodentate or bidentate Ni surface complexes alone resulted in underestimation and overestimation of the Ni sorption respectively. A divalent ion can form both monodentate and bidentate surface species [38]. In the light of the literature it was tested if the model where Ni forms bidentate, and/or monodentate surface complexes with the adsorbent surfaces could explain the experimental data. Hence, in this study we used both monodentate and bidentate Ni surface complex. This is in accordance to previous studies [39,40], that multinuclear Ni surface complexes are formed during Ni adsorption.

The lines in Figs. 2 and 3 show the model fit to experimental data for Ni sorption to different sorbents as a function of pH. The good fit achieved when Ni sorption is represented by reactions (1) and (2) supports the hypothesis that Ni sorption to all four sorbents is dominated by non-specific sorption below pH 6.0, whereas specific sorption to amphoteric aluminol edge sites is the dominating sorption at higher pH values. The model fit for Ni sorption to different sorbents is very satisfactory (Figs. 2 and 3). Gibbsite showed strong Ni adsorption characteristics. Model calculations show that Al sites of gibbsite occupy more surface sites for Ni, than that for laterite, NRE and goethite. However, the decrease in Ni(II) complexation to the goethite surface was possibly due to the less attraction of iron sites on Ni(II) compared to aluminum. This was observed from the model calculations with relevant solution speciation reactions.

### 3.1.2. FTIR results

Molecular vibrations and their changes before and after adsorption can be identified by interpreting the changes of peaks at specified frequencies in IR spectroscopy. Only gibbsite was selected for the IR data interpretation since it showed the highest adsorption compared to other sorbents. In FTIR spectra before and after adsorption, there were clear band shifts and intensity decreases.

For gibbsite, bands at 914, 970 and 1022 cm<sup>-1</sup> (Fig. 4b) correspond to the OH bending vibrations of surface hydroxyl sites [41,42]. Presumably the lower frequency band at 914 cm<sup>-1</sup> is attributed to the Al–O–H group with the least hydrogen bonding influence. The bands in the 500–650 region are overlaps of out-of-plane OH bending vibrations and Al–O vibrations [43]. The peaks observed at 1250–650 cm<sup>-1</sup> are assigned to metal oxide bonds [30].

The deconvolution technique was employed to spectral data in the region of 3000–4000 cm<sup>-1</sup> as the actual number of bands cannot be counted due to lack of symmetry around band centers and consistency of shoulders. Deconvolution resulted in seven bands (peak/full width at height maximum (FWHM)) at 3623/27, 3609/239, 3523/52, 3463/37, 3434/18, 3408/119 and 3287/186 for bare gibbsite (Fig. 4b). Nickel adsorbed gibbsite was reported with seven bands (Fig. 4c), with shifting the bands to lower wave numbers. The bands shaded in Fig. 4 shows shifting of bands to high wave numbers in the metal oxide region of Ni loaded gibbsite, suggesting Ni adsorption onto gibbsite is based on an inner-sphere monodentate bonding mechanism.

## 3.2. Sorption isotherms

### 3.2.1. Isotherm models

The equilibrium relationship between different adsorbents and adsorbate was assessed by two and three parameter isotherm models (Langmuir, Freundlich, Redlich–Peterson, and Hill). The Langmuir and Hill models assume a monolayer adsorption phenomenon on a homogeneous surface [35] while other models (Freundlich, Redlich and Peterson isotherm) represent solute adsorption onto heterogeneous surfaces [19,44] (Fig. 5).

In the Langmuir equation the adsorption density, is expressed as,

$$\Gamma_{\text{ads}} = \frac{\Gamma_{\text{max}} K_L C_e}{1 + K_L C_e} \quad (1)$$

where  $\Gamma_{\text{ads}}$  is the amount of adsorbate adsorbed per unit area of surface (mol m<sup>-2</sup>),  $C_e$  is the equilibrium solution concentration (mol dm<sup>-3</sup>) of adsorbate and  $K_L$  is the equilibrium constant for the overall adsorption process. The Langmuir model assumes that all adsorption sites have equal affinity for the adsorbate and that only monolayer adsorption occurs.

In the Hill model of adsorption, surface is also assumed to be homogeneous and the model given is,

$$\Gamma_{\text{ads}} = \frac{\Gamma_{\text{max}} (K_L C_e)^a}{1 + (K_L C_e)^a} \quad (2)$$

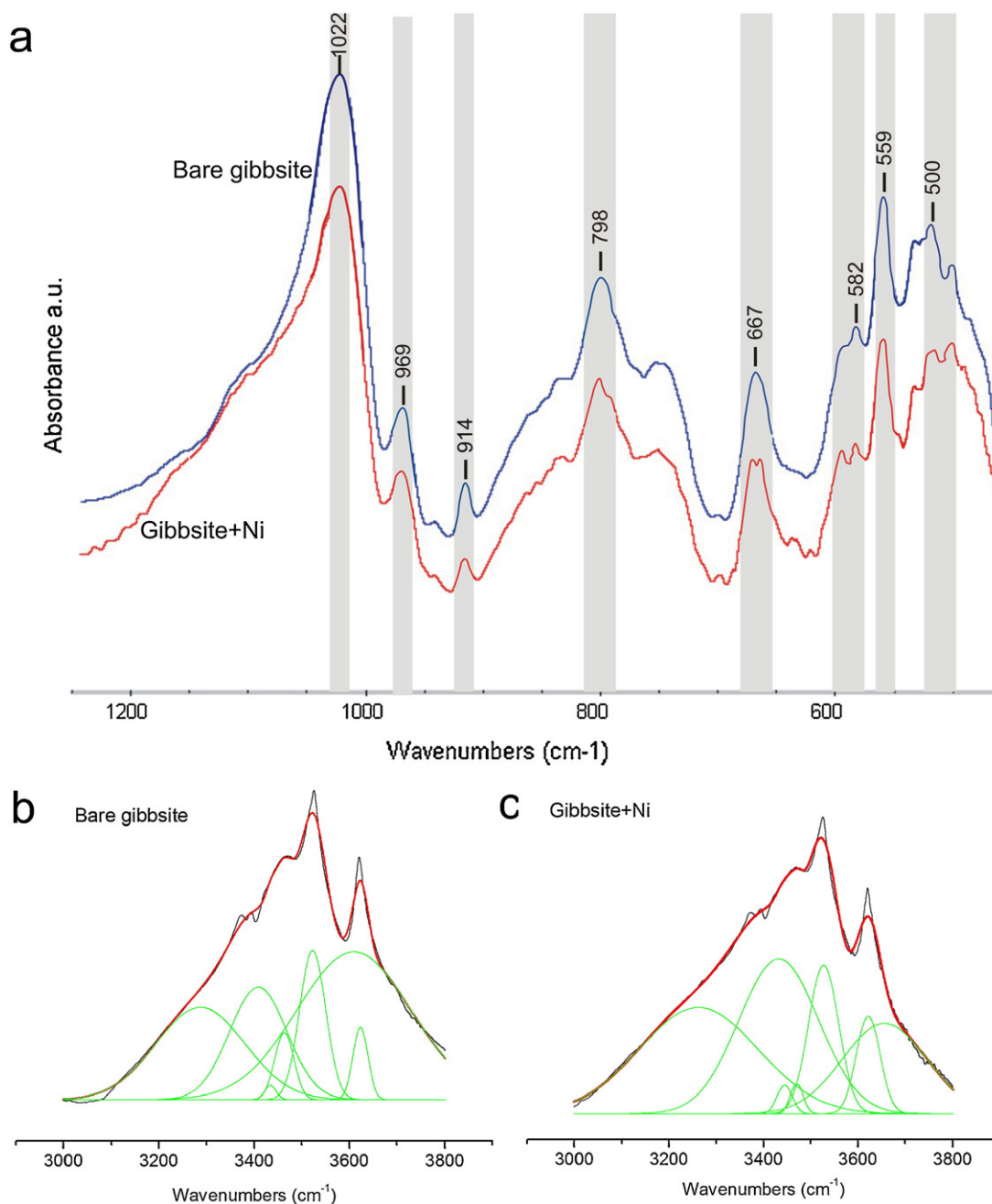


**Fig. 4.** (a) FTIR Spectra of aqueous suspension of bare gibbsite and Ni loaded gibbsite at pH 7 for the region 400–3000  $\text{cm}^{-1}$ ; (b) curve decomposition for bare gibbsite; (c) curve decomposition for Ni loaded gibbsite. Ni was at a concentration of  $1.709 \times 10^{-4}$  M. Suspension concentration of 5 g/L for 0.01 M  $\text{NaNO}_3$ .

where the term definitions shown in the Langmuir model are valid; additionally parameter  $a$  assesses the degree of interactions between adsorbent and adsorbate. For positive interactions,  $a$  should be greater than 1. In this model, the adsorption is treated as a cooperative process due to adsorbate–adsorbent interactions.

The characteristics of the Langmuir isotherm could be expressed in terms of the separation factor or equilibrium parameter,  $K_R$ , a dimensionless constant that indicated whether the adsorption reaction was favorable by the equation [45–47]; where  $K_L$  is the affinity constant estimated by the Langmuir equation (Eq. (1)).

$$K_R = \frac{1}{1 + K_L C_e} \quad (3)$$

Unlike the Langmuir isotherm, the Freundlich isotherm does not imply a maximum adsorption capacity of the sorbent and

Freundlich constant ( $n$ ) can be used to identify favorable adsorptions. In the Freundlich equation, the adsorption density  $\Gamma_{\text{ads}}$  ( $\text{mol m}^{-2}$ ) is given as,

$$\Gamma_{\text{ads}} = K_F C_e^n \quad (4)$$

where  $K_F$  ( $(\text{mol m}^{-2})/(\text{mol dm}^{-3})^n$ ) and  $n$  are Freundlich constants related to adsorption capacity and adsorption intensity.

Redlich–Peterson isotherm is a three-parameter equation to incorporate features of both Langmuir and Freundlich equations and at low concentrations, it approximates to Henry's law and at high concentration its behavior approaches that of the Freundlich isotherm [45].

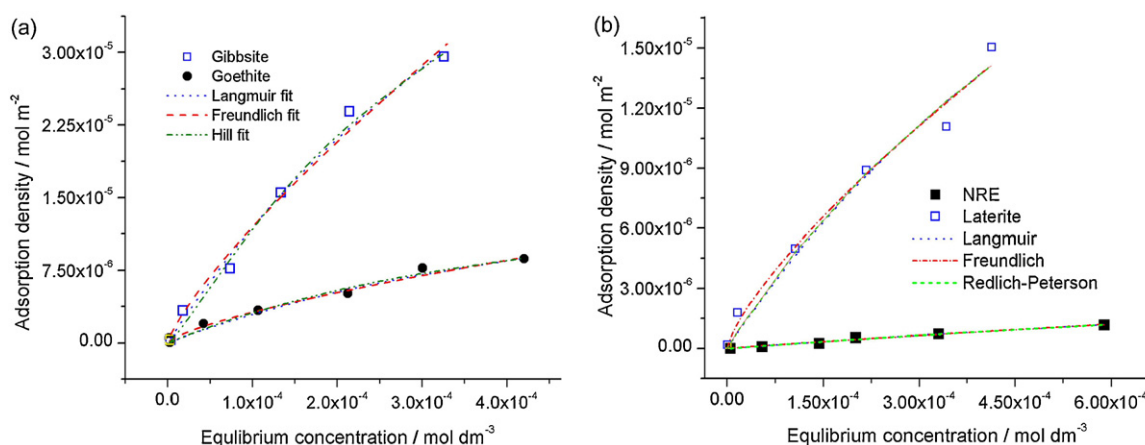


**Fig. 5.** Langmuir, Freundlich and Hill isotherm Ni on four sorbents at 0.01 M NaNO<sub>3</sub>, pH 7.5. Symbols represent experimental results and line represents calculated results using non-linear least square fit.

The Redlich and Peterson isotherm can be expressed as,

$$\Gamma_{\text{ads}} = \frac{\Gamma_{\text{max}} C_e}{1 + a_R C_e^{n_R}} \quad (5)$$

where  $\Gamma_{\text{ads}}$ ,  $\Gamma_{\text{max}}$  and  $C_e$  have the same definitions in Eq. (1),  $a_R$  the Redlich–Peterson isotherm constant ( $\text{dm}^3 \text{mol}^{-1}$ ), and  $n_R$  is the Redlich–Peterson isotherm exponent.

The thermodynamic parameter, Gibb's free energy change,  $\Delta G^\circ$ , was calculated using  $K_L$  obtained from Langmuir equation (Eq. (1)).

$$\Delta G^\circ = -RT \ln K_L;$$

where  $R$  is universal gas constant ( $8.314 \text{ J mol}^{-1} \text{ K}^{-1}$ ) and  $T$  is the absolute temperature in  $K$ .

The isotherm parameters were estimated by fitting to non-linear regression isotherm models and optimized values are detailed in Table 3. For all the adsorbents, all four isotherm models studied, such as the Langmuir, Freundlich, and Redlich–Peterson showed high  $r^2$  values (more than 0.9). It indicates the possibility of simultaneous validity of multiple isotherm models. The estimated values were in agreement with the experimental values and both Langmuir isotherm constant  $K_L$ , and maximum adsorption density,  $q_{\text{max}}$  values for gibbsite are higher than those for goethite, laterite and NRE. The optimized Freundlich constant values and

**Table 3**

Constants for different isotherms used in data modeling.

Langmuir isotherm					
Adsorbate	$\Gamma_{\text{max}}$ ( $\text{mol m}^{-2}$ )	$K_L$ ( $\text{dm}^3 \text{mol}^{-1}$ )	$r^2$	$\chi^2$	
Gibbsite	$9.00 \times 10^{-5}$	$1.58 \times 10^3$	0.992	$1.44 \times 10^{-12}$	
Goethite	$2.00 \times 10^{-5}$	$1.50 \times 10^3$	0.970	$4.07 \times 10^{-13}$	
Laterite	$4.00 \times 10^{-5}$	$1.13 \times 10^3$	0.978	$9.02 \times 10^{-13}$	
NRE	$6.01 \times 10^{-6}$	$4.13 \times 10^2$	0.984	$3.91 \times 10^{-15}$	
Freundlich isotherm					
Adsorbate	$K_F$ ( $\text{mol m}^{-2}$ )/( $\text{dm}^3 \text{mol}^{-1}$ ) <sup>n</sup>	$n$	$r^2$	$\chi^2$	
Gibbsite	$1.81 \times 10^{-2}$	$7.94 \times 10^{-1}$	0.987	$2.12 \times 10^{-12}$	
Goethite	$2.36 \times 10^{-3}$	$7.19 \times 10^{-1}$	0.976	$3.29 \times 10^{-13}$	
Laterite	$5.01 \times 10^{-3}$	$7.53 \times 10^{-1}$	0.984	$6.46 \times 10^{-13}$	
NRE	$9.40 \times 10^{-4}$	$9.00 \times 10^{-1}$	0.987	$4.54 \times 10^{-15}$	
Hill isotherm					
Adsorbate	$\Gamma_{\text{max}}$ ( $\text{mol m}^{-2}$ )	$K_L$ ( $\text{dm}^3 \text{mol}^{-1}$ )	$a$	$r^2$	$\chi^2$
Gibbsite	$5.00 \times 10^{-5}$	$3.81 \times 10^3$	1.27	0.993	$1.61 \times 10^{-12}$
Goethite	$2.00 \times 10^{-5}$	$2.37 \times 10^3$	1.05	0.984	$2.26 \times 10^{-13}$
Redlich and Peterson isotherm					
Adsorbate	$\Gamma_{\text{max}}$ ( $\text{mol m}^{-2}$ )	$a_R$ ( $\text{dm}^3 \text{mol}^{-1}$ )	$n_R$	$r^2$	$\chi^2$
Laterite	$5.30 \times 10^{-2}$	$4.88 \times 10^2$	$8.47 \times 10^{-1}$	0.979	$8.70 \times 10^{-13}$
NRE	$2.52 \times 10^{-3}$	$2.10 \times 10^2$	$9.02 \times 10^{-1}$	0.983	$3.97 \times 10^{-15}$
Adsorbate	$\Delta G^\circ$ ( $\text{kJ mol}^{-1}$ )				
Gibbsite	−18.2				
Goethite	−18.1				
Laterite	−17.4				
NRE	−14.9				

Note:  $r^2$  represents correlation coefficient and chi-square ( $\chi^2$ ) represents the goodness of fit.

calculated Langmuir separation factors show that the Ni adsorption is favorable for all adsorbents ( $0 < n < 1$  and  $0 < K_R < 1$ ) (Table 3). The negative values of  $\Delta G^\circ$  confirm the feasibility of the process and the spontaneous nature of adsorption with all the sorbents. Among all the adsorption isotherm models studied here, the Hill adsorption isotherm present the best fit with the experimental data of the gibbsite and goethite systems suggesting the homogeneous adsorption behavior. Freundlich isotherm shows the best fit for other two systems which have both Al and Fe sites (dual sites) where sorption affinity varies as higher-affinity sites are filled and more abundant lower-affinity sites become dominant. Among all the sorbents, gibbsite has the maximum adsorption capacity and this finding corroborates with the SEM data which suggests the preference of Ni to  $\equiv\text{Al}$  sites rather than  $\equiv\text{Fe}$  sites.

#### 4. Conclusion

Ni showed a strong affinity for gibbsite and laterite forming inner-sphere surface complexes. The Ni adsorption was modeled successfully using binding constants derived for single and dual sorbate systems. Given the relative concentration of the adsorbent and their affinity to nickel, the adsorption behavior of all four adsorbents were successfully interpreted with a mechanistic model based on the parameters obtained from the sorption data of single and dual site clays. However, the highest affinity was shown by gibbsite and thereafter laterite. Both Hill and Freundlich isotherms yield good fits and the adsorption coefficients agree well with the conditions supporting favorable adsorption. The results indicate that Ni has a better affinity to aluminum surface than to iron surfaces.

#### Acknowledgments

Authors would like to thank Prof. T. Pradeep and Dr. Sajan Lal at the DST Unit of Nanoscience, Indian Institute of Technology, Chennai for providing SEM results. International Foundation for Science (IFS, Sweden) is kindly acknowledged for their grant (Grant Number: W/5068-1) given to support this study. Reviewers and editorial comments helped to improve the manuscript quality and clarity.

#### References

- [1] C.H. Cheng, S.H. Jien, Y. Iizuka, H. Tsai, Y.H. Chang, Z.Y. Hseu, Pedogenic chromium and nickel partitioning in serpentine soils along a toposequence, *Soil Sci. Soc. Am. J.* 75 (2011) 659–668.
- [2] J. Kierczak, C. Neel, H. Bril, J. Puziewicz, Effect of mineralogy and pedoclimatic variations on Ni and Cr distribution in serpentine soils under temperate climate, *Geoderma* 142 (2007) 165–177.
- [3] C. Oze, S. Fendorf, D.K. Bird, R.G. Coleman, Chromium geochemistry of serpentine soils, *Int. Geol. Rev.* 46 (2004) 97–126.
- [4] R.G. Crouse, W.J. Pories, J.T. Bray, R.L. Mauger, Geochemistry and man: health and disease. 1. essential elements. 2. Elements possibly essential, those toxic and others, in: I. Thornton (Ed.), *Applied Environmental Geochemistry*, Academic Press, London, 1983, pp. 267–333.
- [5] M. Piscator, The dependence of toxic reactions on the chemical species of elements, in: M. Bernhard, F.E. Brinckman, P.J. Sadler (Eds.), *The Importance of Chemical 'Speciation' in Environmental Processes*, Springer-Verlag, 1986.
- [6] K. Kadirvelu, K. Thamaraiselvi, C. Namasivayam, Adsorption of nickel(II) from aqueous solution onto activated carbon prepared from coirpith, *Sep. Purif. Technol.* 24 (2001) 497–505.
- [7] A.K. Meena, G.K. Mishra, P.K. Rai, C. Rajagopal, P.N. Nagar, Removal of heavy metal ions from aqueous solutions using carbon aerogel as an adsorbent, *J. Hazard. Mater.* 122 (2005) 161–170.
- [8] K.G. Bhattacharyya, S.S. Gupta, Adsorption of a few heavy metals on natural and modified kaolinite and montmorillonite: a review, *Adv. Colloid Interface Sci.* 140 (2008) 114–131.
- [9] X. Gu, L.J. Evans, Surface complexation modelling of Cd(II), Cu(II), Ni(II), Pb(II) and Zn(II) adsorption onto kaolinite, *Geochim. Cosmochim. Acta* 72 (2008) 267–276.
- [10] Ö. Yavuz, Y. Altunkaynak, F. Güzel, Removal of copper, nickel, cobalt and manganese from aqueous solution by kaolinite, *Water Res.* 37 (2003) 948–952.
- [11] X. Gu, L.J. Evans, S.J. Barabash, Modeling the adsorption of Cd(II), Cu(II), Ni(II), Pb(II) and Zn(II) onto montmorillonite, *Geochim. Cosmochim. Acta* 74 (2010) 5718–5728.
- [12] N. Boujelben, J. Bouzid, Z. Elouear, Adsorption of nickel and copper onto natural iron oxide-coated sand from aqueous solutions: study in single and binary systems, *J. Hazard. Mater.* 163 (2009) 376–382.
- [13] J.P. Beukes, E.W. Giesekke, W. Elliott, Nickel retention by goethite and hematite, *Miner. Eng.* 13 (2000) 1573–1579.
- [14] Z.-r. Liu, X.-s. Chen, L.-m. Zhou, P. Wei, Development of a first-order kinetics-based model for the adsorption of nickel onto peat, *Mining Sci. Technol. (China)* 19 (2009) 230–234.
- [15] Z.-r. Liu, S.-q. Zhou, Adsorption of copper and nickel on Na-bentonite, *Process Saf. Environ. Prot.* 88 (2010) 62–66.
- [16] H.-r. Wu, C.-I. Lin, L.-H. Wang, Effect of peanut hull ash dosage on the degree of influence of operation variables on the adsorption of nickel ion from aqueous solution using peanut hull ash, *J. Taiwan Inst. Chem. Eng.* 42 (2011) 658–661.
- [17] Y. Alvarado-Ibarra, F. Granados-Correa, V.H. Lara, P. Bosch, S. Bulbulian, Nickel(II) sorption on porous ZnO prepared by solution combustion method, *Colloids Surf. Physicochem. Eng. Aspects* 345 (2009) 135–140.
- [18] P.M. Choksi, V.Y. Joshi, Adsorption kinetic study for the removal of nickel(II) and aluminum(III) from an aqueous solution by natural adsorbents, *Desalination* 208 (2007) 216–231.
- [19] V.C. Srivastava, I.D. Mall, I.M. Mishra, Competitive adsorption of cadmium(II) and nickel(II) metal ions from aqueous solution onto rice husk ash, *Chem. Eng. Process.: Process Intensification* 48 (2009) 370–379.
- [20] H. Green-Pedersen, B.T. Jensen, N. Pind, Nickel adsorption on  $\text{MnO}_2$ ,  $\text{Fe}(\text{OH})_3$ , montmorillonite, humic acid and calcite: a comparative study, *Environ. Technol.* 18 (1997) 807–815.
- [21] S.S. Gupta, K.G. Bhattacharyya, Adsorption of Ni(II) on clays, *J. Colloid Interface Sci.* 295 (2006) 21–32.
- [22] J. Echeverria, J. Indurain, E. Churio, J. Garrido, Simultaneous effect of pH, temperature, ionic strength, and initial concentration on the retention of Ni on illite, *Colloids Surf. Physicochem. Eng. Aspects* 218 (2003) 175–187.
- [23] H. Marcussen, P.E. Holm, B.W. Strobel, H.C.B. Hansen, Nickel sorption to goethite and montmorillonite in presence of citrate, *Environ. Sci. Technol.* 43 (2009) 1122–1127.
- [24] D.A. Palmer, S.Y. Shiao, R.E. Meyer, J.A. Wethington, Adsorption of nuclides on mixtures of minerals, *J. Inorg. Nucl. Chem.* 43 (1981) 3317–3322.
- [25] C.L. Peacock, D.M. Sherman, Vanadium(V) adsorption onto goethite ( $\alpha\text{-FeOOH}$ ) at pH 1.5–12: a surface complexation model based on ab initio molecular geometries and EXAFS spectroscopy, *Geochim. Cosmochim. Acta* 68 (2004) 1723–1733.
- [26] J. Westall, H. Hohl, A comparison of electrostatic models for the oxide/solution interface, *Adv. Colloid Interface Sci.* 12 (1980) 265–294.
- [27] D.A. Dzombak, F.M.M. Morel, Sorption of cadmium on hydrous ferric oxide at high sorbate/sorbent ratios: equilibrium, kinetics, and modeling, *J. Colloid Interface Sci.* 112 (1986) 588–598.
- [28] T. Hiemstra, J.C.M. De Wit, W.H. Van Riemsdijk, Multisite proton adsorption modeling at the solid/solution interface of (hydr)oxides: a new approach: II. Application to various important (hydr)oxides, *J. Colloid Interface Sci.* 133 (1989) 105–117.
- [29] K. Dahanayake, S.K. Jayawardana, Study of red and brown earth deposits of north-west Sri Lanka, *J. Geol. Soc. India* 20 (1979) 433–440.
- [30] M. Vithanage, R. Chandrajith, A. Bandara, R. Weerasooriya, Mechanistic modeling of arsenic retention on natural red earth in simulated environmental systems, *J. Colloid Interface Sci.* 294 (2006) 265–272.
- [31] M. Vithanage, W. Senevirathna, R. Chandrajith, R. Weerasooriya, Arsenic binding mechanisms on natural red earth: a potential substrate for pollution control, *Sci. Total Environ.* 379 (2007) 244–248.
- [32] M.K.R. Chowdhury, V. Venketesh, M.A. Anandalwar, D.K. Paul, Recent Concepts on the Origin of Indian Laterite, *Geological Survey of India*, vol. 31, Calcutta, 1965, pp. 547–558.
- [33] Y. Tardy, Petrology of Laterites and Tropical Soils, A.A. Balkema, Netherlands, 1997.
- [34] M. Vithanage, L. Jayarathna, A.U. Rajapaksha, C.B. Dissanayake, M.S. Bootharaju, T. Pradeep, Modeling sorption of fluoride on to iron rich laterite, *Colloids Surf. Physicochem. Eng. Aspects* 398 (2012) 69–75.
- [35] W. Stumm, J.J. Morgan, *Chemical equilibria and rates in natural waters*, in: *Aquatic Chemistry*, Wiley Interscience, 1996.
- [36] S. Mattigod, D. Rai, A. Felmy, L. Rao, Solubility and solubility product of crystalline Ni(OH)<sub>2</sub>, *J. Solution Chem.* 26 (1997) 391–403.
- [37] K.F. Hayes, C. Pappas, J.O. Leckie, Modeling ionic strength effects on anion adsorption at hydrous oxide/solution interfaces, *J. Colloid Interface Sci.* 125 (1988) 717–726.
- [38] P. Venema, T. Hiemstra, W.H. van Riemsdijk, Multisite adsorption of cadmium on goethite, *J. Colloid Interface Sci.* 183 (1996) 515–527.
- [39] Y. Arai, Spectroscopic evidence for Ni(II) surface speciation at the iron oxyhydroxides-water interface, *Environ. Sci. Technol.* 42 (2008) 1151–1156.
- [40] M.J. Eick, S.E. Fendorf, Reaction sequence of nickel(II) with kaolinite: mineral dissolution and surface complexation and precipitation, *Soil Sci. Soc. Am. J.* 62 (1998) 1257–1267.
- [41] C.K. Kumara, W.J. Ng, A. Bandara, R. Weerasooriya, Nanogibbsite: synthesis and characterization, *J. Colloid Interface Sci.* 352 (2010) 252–258.
- [42] J.D. Russell, R.L. Parfitt, A.R. Fraser, V.C. Farmer, Surface structures of gibbsite goethite and phosphated goethite, *Nature* 248 (1974) 220–221.

- [43] T. Takamura, J. Koezuka, Infra-red evidence of the grinding effect on hydrargillite single crystals, *Nature* 207 (1965) 965–966.
- [44] R. Weerasooriya, H.K.D.K. Wijesekara, A. Bandara, Surface complexation modeling of cadmium adsorption on gibbsite, *Colloids Surf. Physicochem. Eng. Aspects* 207 (2002) 13–24.
- [45] Y.S. Ho, J.F. Porter, G. McKay, Equilibrium isotherm studies for the sorption of divalent metal ions onto peat: copper, nickel and lead single component systems, *Water Air Soil Pollut.* 141 (2002) 1–33.
- [46] M. Mahramanlioglu, I. Kizilcikli, I.O. Bicer, Adsorption of fluoride from aqueous solution by acid treated spent bleaching earth, *J. Fluorine Chem.* 115 (2002) 41–47.
- [47] T.S. Singh, K.K. Pant, Equilibrium, kinetics and thermodynamic studies for adsorption of As(III) on activated alumina, *Sep. Purif. Technol.* 36 (2004) 139–147.
- [48] A. Herbelin, J.C. Westall, FITEQL 3.1, A computer program for determination of chemical equilibrium constants from experimental data, Department of Chemistry, Oregon State University, 1994.
- [49] A. Richter, V. Brendler, C. Nebelung, Blind prediction of Cu(II) sorption onto goethite: current capabilities of diffuse double layer model, *Geochim. Cosmochim. Acta* 69 (2005) 2725–2734.